Supporting Information for Publication

The Influence of Gas Phase Equilibria on the Chemical Vapor Deposition of Graphene

*Amanda M. Lewis, Brian Derby, Ian A. Kinloch**

[1]School of Materials, University of Manchester, Grosvenor Street, M13 9PL

Table S1. Classifications and experimental conditions for graphene deposition in the literature, showing the carbon to hydrogen ratio used (R_{CH}), reaction temperature and pressure (T_r and P_r), the total pressure of hydrocarbons plus hydrogen in the system (P_A).

Deposition Type	R_{CH}	T_r, °C	P_r, mbar	P_A, mbar	**Reference**
Few Layer	0.0050	975	1013	1013	[1]
	0.0294	1000	2.0	2.0	[2]
	0.0455	975	1013	1013	[1]
	0.2500	1000	1013	81	[3]
	0.2500	1000	1013	48	[2]
	0.4286	950	0.67	0.67	[4]
Bilayer	0.2500	1000	0.67	0.67	[2]
Decorated monolayer	0.0021	1050	1013	13	[5]
	0.0108	1000	1013	1013	[6]
	0.0179	1050	1013	14	[5]

	0.0381	1000	1013	1013	[6]
	0.0938	1060	1013	13	[7]
	0.0950	1000	1013	22	[8]
	0.1923	1070	1013	162	[9]
	0.2000	1030	1013	182	[9]
	0.2000	1050	1013	182	[9]
	0.2000	1070	1013	182	[9]
	0.2016	1000	1013	50	[8]
	0.2174	1000	1013	62	[10]
	0.2174	1050	1013	62	[11]
	0.2415	1000	1013	205	[8]
Defective monolayer	0.0049	1000	1013	17	[8]
	0.0227	1000	1013	17	[8]
	0.2000	900	1013	61	[12]
	0.3333	750	13	0.78	[13]
	0.3333	830	13	0.78	[13]
Monolayer	0.0004	1050	1013	13	[5]
	0.0008	1050	1013	13	[5]
	0.0011	1000	1013	33	[14]
	0.0011	1050	1013	13	[5]
	0.0012	1000	1013	17	[8]
	0.0096	1000	1013	103	[6]
	0.0185	1000	1013	105	[6]
	0.0694	1000	1013	29	[13]
	0.0714	1000	1013	24	[12]

	0.1207	1000	0.83	0.83	[6]
	0.1818	1050	1013	142	[9]
	0.1818	1070	1013	142	[9]
	0.1923	1050	1013	162	[9]
	0.2000	1000	1013	101	[6]
	0.2059	850	4.1	0.073	[15]
	0.2134	1000	13	13	[16]
	0.2143	1000	0.61	0.61	[17]
	0.2222	1000	10	10	[18]
	0.2381	1050	0.67	0.67	[19]
	0.2431	1000	0.67	0.67	[20]
	0.2453	1000	7.3	7.3	[21]
	0.2500	1000	1013	6.7	[3]
Interrupted monolayer	0.0002	1050	1013	13	[5]
	0.2381	950	0.67	0.67	[19]
Isolated Islands	0.0014	1000	0.47	0.47	[22]
	0.0024	1000	0.27	0.27	[22]
	0.0065	1000	1013	252	[23]
	0.0111	1000	1013	1013	[24]
	0.0111	1025	1013	1013	[24]
	0.0294	1000	1013	1013	[24]
	0.0417	1000	1013	1013	[24]
	0.0625	1000	1013	1013	[24]
	0.0625	900	1013	1013	[24]
	0.1000	800	1013	1013	[24]

	0.1667	1000	0.80	0.80	[24]
	0.1775	1000	1013	0.056	[22]
	0.2021	1000	1013	0.046	[22]
	0.2188	1035	0.26	0.26	[25]
	0.2302	1000	1013	0.036	[22]
	0.2337	1035	0.43	0.43	[25]
	0.2381	975	0.67	0.67	[19]
	0.2381	900	0.67	0.67	[19]
	0.2431	950	0.67	0.67	[26]
	0.6688	300	0.89	0.89	[27]
	0.6688	400	0.89	0.89	[27]
	0.6688	500	0.89	0.89	[27]
	0.6688	600	0.89	0.89	[27]
None	0.1818	1030	1013	142	[9]
	0.1923	1030	1013	162	[9]
	0.2174	950	1013	62	[11]
	0.2222	750	4.1	0.076	[15]
	0.2397	1000	1013	0.034	[22]

Raman Spectroscopy

Raman spectra were collected from graphene *in situ* on the copper substrate at an excitation wavelength of 514 nm, and are presented in Figure S1. The spectra have been normalized to the intensity of the G peak and offset. The background comes from the fluorescence of the copper.

The majority of samples display a clean graphene Raman signature, with no D peak. The spectrum with the narrowest, most intense G' peak was collected from a sample produced at the

lowest pressure, 0.001 mbar, and highest temperature, 1040 °C, used for deposition. As the pressure was increased and the temperature reduced, the G' peak broadens and its intensity reduces. For the lowest deposition temperatures and pressures used, the graphene islands are sparse and no Raman signal is seen.

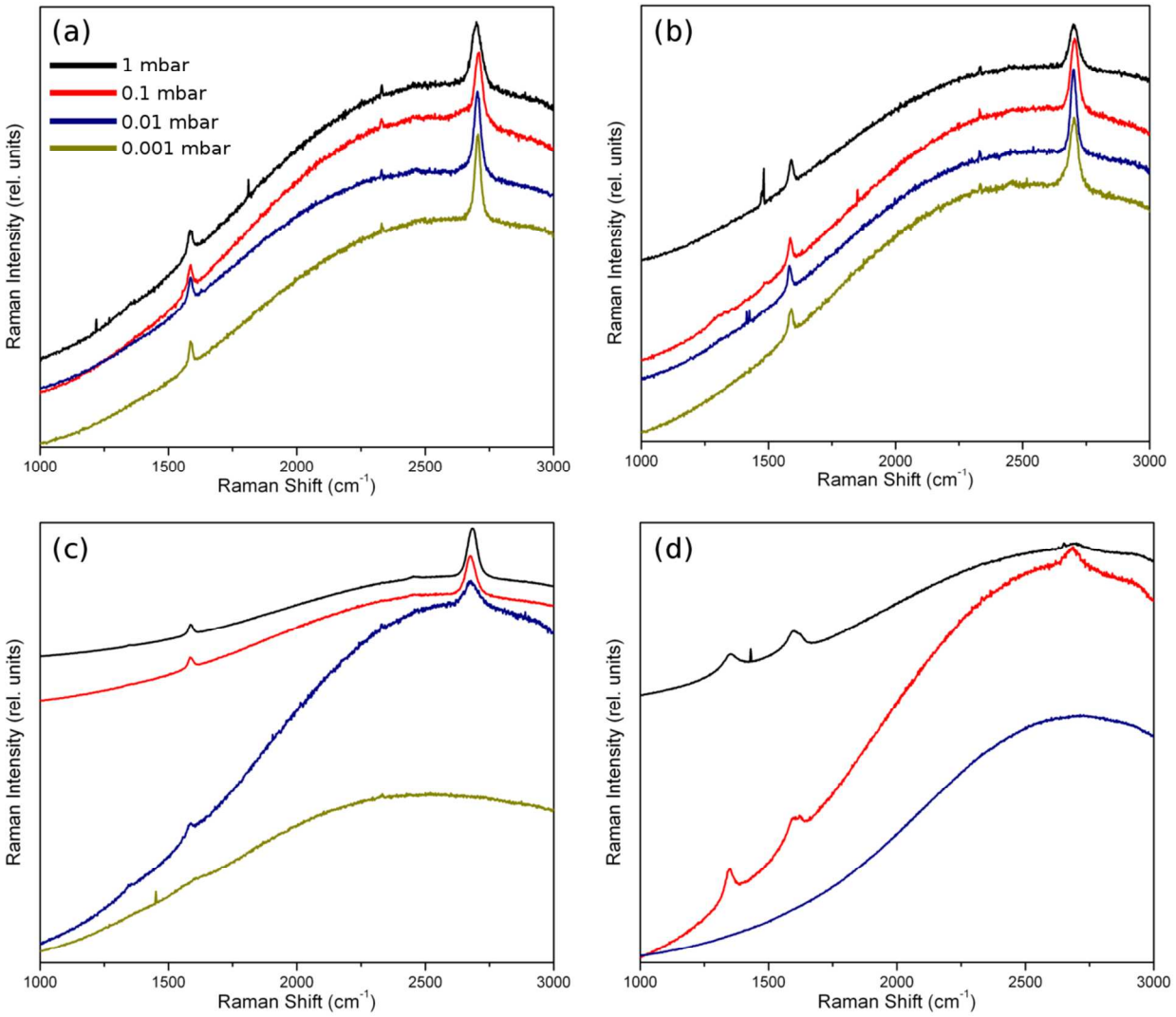

Figure S1. Raman spectra of the graphene deposited at a temperature of (a) 1040 °C, (b) 916 °C, (c) 816 °C and (d) 716 °C. Line color indicates the deposition pressure as follows: Black, 1 mbar; red, 0.1 mbar; navy, 0.01 mbar; dark yellow, 0.001 mbar.

Scanning Electron Microscopy (SEM) of Sooty Deposits

Several of the samples discussed in this study exhibited areas of low secondary electron emission in the SEM micrographs, collected using a through-lens detector which provides ultra-high resolution (Figure SI 2 (a)). Higher magnification scans revealed that these areas have an amorphous, scrolled texture (Figure S2 (a) - inset), indicating that soot had been deposited on the graphene film or the underlying copper. Micrographs were collected from the same sample using both the through lens detector with ultra high resolution (Figure S2 (b)) and the standard secondary electron detector (Figure S2 (c)). This comparison of the two detectors revealed that the sooty deposits are not clear when operating outside of the ultra high resolution mode.

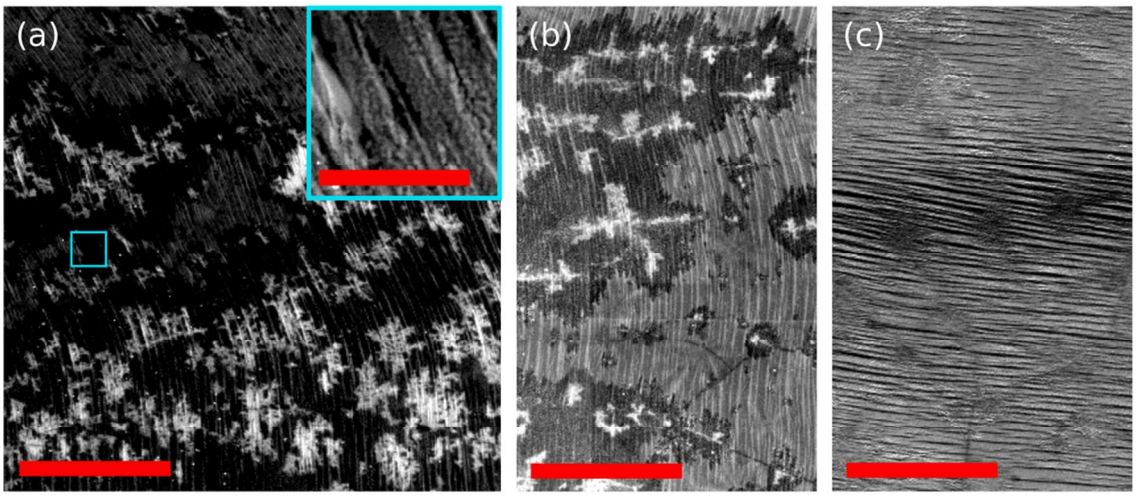

Figure S2. SEM micrographs of a graphene sample *in situ* on the copper substrate grown at a temperature of 1040 °C and a pressure of 1 mbar. (a) low magnification image, showing graphene coverage (mid tone, stepped regions) and sooty deposits. Scale bar: 10 µm. Inset: higher magnification micrograph of same area. Scale bar: 2 µm. Images of similar ares of the sample taken using (b) ultra-high resolution with the through-lens detector and (c) the standard secondary electron detector Scale bars: 10 µm.

The Calculation of Flow Parameters and their Influence on the Model

The dimensionless Reynolds number, $Re(L)$, indicates flow through a pipe is laminar when $Re(L) < 2300$ [28] and turbulent otherwise and is calculated using equation S1,

$$Re(L) = \frac{\rho v L}{\mu} \qquad \text{S1}$$

where ρ is the gas density, v is the mean velocity of the flow, L is set to the pipe radius, r, and μ is the dynamic viscosity. We use the ideal gas model and the principle of conservation of mass to convert the volumetric flow rate at which gases are introduced to the chamber, V_s, to that expected within the chamber, V_r, and divide by the cross-sectional pipe area to calculate v so that in terms of the reaction pressure P_r and temperature T_r,

$$v = \frac{V_r}{\pi r^2} = \frac{V_S P_S T_r}{T_S P_r \pi r^2} . \qquad \text{S2}$$

We assume that V_s is measured at standard temperature and pressure, so that T_s = 293.15 K and P_s = 1013.25 mbar. The gas density is calculated using the ideal gas law to determine the concentration per unit volume of molecules within the reaction chamber and multiplying by the molecular mass, m, as shown in equation S3,

$$\rho = \frac{P_r m}{k_B T_r} , \qquad \text{S3}$$

where k_B is Boltmann's constant. The dynamic viscosity is related to the temperature and molecular properties of a given species of gas according to equation S4, [29]

$$\mu = \frac{2}{3\pi^2 d^2}\sqrt{\pi m k_B T_r} , \qquad \text{S4}$$

where d is the molecular diameter. By combining equations S1 to S4 we see that the Reynolds number is dependent only on the flow velocity and temperature for a given chemical and reactor geometry, and is independent of the reaction pressure,

$$Re(L = r) = \frac{3V_s P_s d^2}{2T_s r}\sqrt{\frac{\pi m}{{k_B}^3 T_r}}. \qquad \text{S5}$$

The Reynolds numbers for graphene CVD are listed in Table S2 and show that laminar flow is expected across the entire parameter space.

Table S2. Reynolds number ($Re(r)$), average boundary layer thickness $<\delta(L_s)>$, mean free path (λ), Knudsen number (Kn) and residence time (τ) for CVD of graphene.

P_r, mbar	T_r, °C	Vs, sccm	$Re(r)$		$<\delta(Ls)>$, cm		λ, cm		Kn		τ, ms	Ref.
			H_2	C_2H_2	H_2	C_2H_2	H_2	C_2H_2	H_2	C_2H_2		
APCVD conditions												
							Viscous flow					
1013	1050	1500	5.2	57 (CH_4)	1.4	0.42 (CH_4)	5.1×10^{-5}	1.7×10^{-5} (CH_4)	2.3×10^{-5}	7.5×10^{-6} (CH_4)	1700	[5]
1013	1000	300	1.1	6.5	3.1	1.2	4.9×10^{-5}	2.2×10^{-5}	4.4×10^{-5}	2.2×10^{-5}	8750	[24]
13	830	255	1.0	11	3.2	0.9	0.0032	0.0011	0.0015	4.8×10^{-4}	160	[13]
LPCVD conditions												
							Viscous flow					
1	1040	129	0.45	4.9	4.7	1.4	0.050	0.016	0.02	0.007	20	
1	916	129	0.47	5.2	4.6	1.4	0.046	0.015	0.02	0.007	21	
1	816	129	0.49	5.4	4.5	1.4	0.041	0.014	0.02	0.006	24	
1	716	129	0.52	5.7	4.4	1.3	0.038	0.012	0.02	0.006	26	
1	616	129	0.54	6.0	4.3	1.3	0.034	0.011	0.02	0.005	29	

									Transition flow		
0.1	1040	6	0.023	0.26	21	6.2	0.50	0.16	0.2	0.07	38
0.1	916	6	0.025	0.27	20	6.1	0.46	0.15	0.2	0.07	42
0.1	816	6	0.026	0.28	20	6.0	0.41	0.14	0.2	0.06	45
0.1	716	6	0.027	0.30	19	5.8	0.38	0.12	0.2	0.06	50
0.1	616	6	0.028	0.31	19	5.7	0.34	0.11	0.2	0.05	56
									Molecular flow		
0.01	1040	6.75	0.021	0.23	22	6.6	5.0	1.6	2.3	0.7	4
0.01	916	6.75	0.022	0.24	22	6.5	4.6	1.5	2.0	0.7	5
0.01	816	6.75	0.023	0.26	21	6.3	4.2	1.4	1.9	0.6	5
0.01	716	6.75	0.024	0.26	21	6.2	3.8	1.2	1.7	0.6	6
0.01	616	6.75	0.025	0.28	20	6.0	3.4	1.1	1.5	0.5	6
									Molecular flow		
0.001	1040	3	0.010	0.11	31	9.4	50	16	23	7.4	1
0.001	916	3	0.011	0.12	30	9.1	45	15	21	6.7	1
0.001	816	3	0.011	0.13	30	8.9	42	14	19	6.2	1

0.001	716	3	0.012	0.13	29	8.7	38	12	17	5.6	1
0.001	616	3	0.013	0.14	28	8.5	34	11	16	5.0	1

For all calculations, our reactor geometry has been used so that L_s = 1 cm, r = 1.1 cm and L_{HZ} = 50 cm.

The chance of achieving equilibrium and subsequently the molecules which impinge on the growth substrate depends on whether the system is under molecular or viscous flow, as determined by the Knudsen number, $Kn = \lambda/(2r)$. [28] The mean free path, λ, is determined by the likelihood of collisions between molecules according to their concentration, c, and molecular diameter, [29]

$$\lambda = \frac{1}{\sqrt{2}\pi d^2 c} . \qquad \text{S6}$$

Applying the ideal gas model to equation S6 allows the mean free path to be calculated for reaction conditions,

$$\lambda = \frac{k_B T_r}{\sqrt{2}\pi d^2 P_r} . \qquad \text{S7}$$

When $Kn < 0.01$, inter-molecular collisions are more frequent than collisions with the chamber wall and modeling the fluid as a continuum of viscous packets is reasonable. The Knudsen numbers given in Table S2 show that only system pressures of 1 mbar or greater lead unambiguously to viscous flow. When the system pressure is < 0.1 mbar, the gas phase will be in the molecular flow regime. We note that whilst the bulk of the published data on the CVD of graphene (Table S1) uses chamber pressures where the continuum approximation and a viscous gas model is appropriate, our experimental data at lower chamber pressures may be in the molecular flow regime and the conditions for two distinct regions of equilibrium may no longer be valid.

The boundary layer thickness is typically calculated using equation 1 from the main text. This equation assumes a continuum model for flow, so is inappropriate for $P_r < 0.1$ mbar as just discussed. The average boundary layer thickness for the higher pressures is given in Table S2

and consistently exceeds the chamber radius. This is clearly incorrect and arises because equation 1 assumes an infinite height of gas above the substrate, whereas in a sufficiently narrow tube the flow characteristics are constrained by the tube geometry and δ(x) rapidly converges to *r*. For such deep boundary layers, the linear approximation of the parabolic concentration gradient between the two regimes is an oversimplification. The simplified model of mass transport across a fixed thickness of gas using Fick's first law no longer applies and any solution of the diffusion equation (if indeed this is appropriate) will show a transition from Case 1 to 2. Case 1 now represents an upper limit for the gas-only phase composition above the substrate, which is expected to be strongly influenced by species evolving in Case 2. However, Case 1 can develop in the region of the hot zone upstream of the copper substrate so that species produced in the gas phase are able to diffuse to the substrate, so can still influence deposition when $P_r > 0.01$ mbar.

The Extent of the Environment which Attains Equilibrium

In order to understand if equilibrium is attained under experimental conditions, one needs to consider the residence time of the feedstock gases, τ, compared to time-resolved empirical measurements of chemical composition under corresponding conditions. Residence times are calculated by dividing the length of the isothermal zone of the reactor, L_{HZ}, by the mean flow velocity given in equation S2, so that

$$\tau = \frac{L_{HZ} T_s P_r \pi r^2}{V_s P_s T_r} \qquad \text{S8}$$

Residence times presented in Table S2 are calculated using equation S8 and range from 1 ms to 56 ms for the LPCVD samples prepared in this work, rising to 8.7 s for APCVD reported in the literature. The time taken to reach equilibrium varies with the temperature, pressure and

initial composition of the system, [30] and as such the extent to which equilibrium is reached can only be approximated when there is no directly corresponding literature. Olsvik *et al.* report that the conversion rate of methane improves with increasing temperature and is inhibited by the presence of hydrogen. [31] At 1200 °C, 1 bar and with a feedstock supply of CH_4:H_2 = 1:2, approximately 1 % of the methane will decompose over 50 ms, rising to 20 % after 0.5 s. [31] We expect the reduced hydrogen concentration used in our experiments to improve the conversion rate, [31] whilst the lower pressures and temperatures used for LPCVD will impair it, [30,31] so that approximately 1 % of the CVD environment attains the equilibrium composition in Case 1 for P_r > 0.1 mbar and T_r > 900 °C. For lower temperatures and pressures the reaction progress is expected to be further reduced as the molecular flow regime is encroached. The longer residence times for APCVD will improve the conversion so that over 20 % of the environment develops Case 1 equilibrium. [31] For Case 2, the development of equilibrium will be enhanced by both the proposed catalytic effect of the copper surface, and the no-slip condition at the substrate for viscous flow conditions which extends residence times towards infinity.

The Conversion of Introduced Carbon to Graphene

The apparently low decomposition rate of methane in LPCVD becomes significant when compared with the conversion rate of carbon to graphene in the hot-walled CVD furnace. Over a typical reaction time of 30 mins and with the lowest methane flow used of 1 sccm, 30 cm^3 = $3x10^{-5}$ m^3 of methane (measured at STP) passes through the furnace, containing $7.5x10^{20}$ carbon atoms. A graphene film has $2.9x10^{19}$ carbon atoms per metre squared, so for a 1 cm^2 substrate completely covered by graphene there are $2.9x10^{15}$ carbon atoms, 0.0003 % of those available from the gas feedstock. Therefore even if only 0.1 % of the feedstock gas reaches equilibrium,

that equilibrium composition still contains over 250 times the amount of carbon required to form the graphene film. In this scenario, the methane could be acting as a "carrier gas" for the products of its decomposition.

Case 1 Equilibria for Other R_{CH}

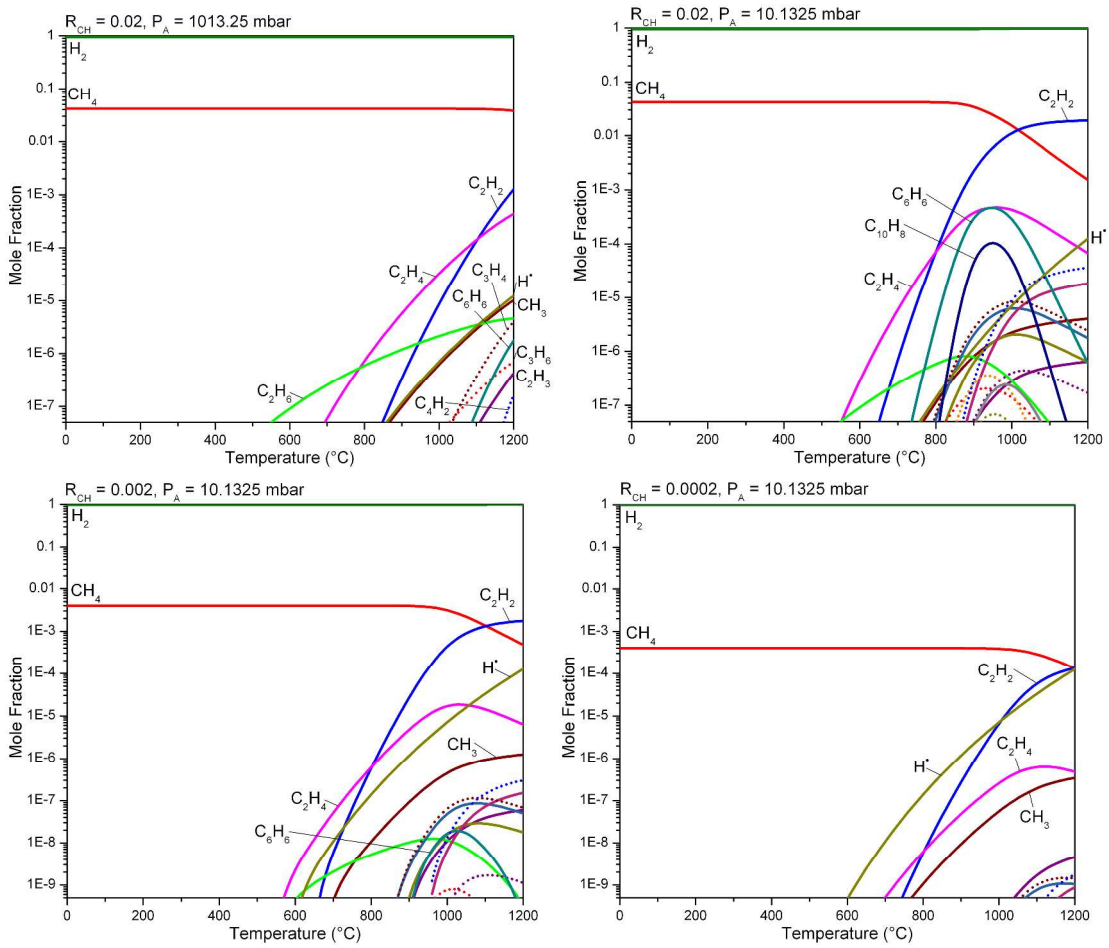

Figure S3: Case 1 equilibria for typical APCVD parameters showing the effect of reducing PA below Pr and the effect of varying RCH on the compositions: (a) R_{CH} = 0.02, P_A = 1013.25 mbar; (b) R_{CH} = 0.02, P_A = 10.1325 mbar; (c) R_{CH} = 0.002, P_A = 10.1325 mbar; (d) R_{CH} = 0.0002, P_A = 10.1325 mbar.

REFERENCES

1. Yao, Y.; Li, Z.; Lin, Z.; Moon, K.-S.; Agar, J.; Wong, C. Controlled Growth of Multilayer, Few-Layer, and Single-Layer Graphene on Metal Substrates. *J. Phys. Chem. C* **2011**, *115*, 5232–5238.

2. Lee, S.; Lee, K.; Zhong, Z. Wafer Scale Homogeneous Bilayer Graphene Films by Chemical Vapor Deposition. *Nano Lett.* **2010**, *10*, 4702–4707.

3. Diaz-Pinto, C.; De, D.; Hadjiev, V. G.; Peng, H. AB-stacked Multilayer Graphene Synthesized *via* Chemical Vapor Deposition: a Characterization by Hot Carrier Transport. *ACS Nano* **2012**, *6*, 1142–1148.

4. Srivastava, A.; Galande, C.; Ci, L.; Song, L.; Rai, C.; Jariwala, D.; Kelly, K. F.; Ajayan, P. M. Novel Liquid Precursor-Based Facile Synthesis of Large-Area Continuous, Single, and Few-Layer Graphene Films. *Chem. Mater.* **2010**, *22*, 3457–3461.

5. Wu, W.; Yu, Q.; Peng, P.; Liu, Z.; Bao, J.; Pei, S.-S. Control of Thickness Uniformity and Grain Size in Graphene Films for Transparent Conductive Electrodes. *Nanotechnology* **2012**, *23*, 035603.

6. Bhaviripudi, S.; Jia, X.; Dresselhaus, M. S.; Kong, J. Role of Kinetic Factors in Chemical Vapor Deposition Synthesis of Uniform Large Area Graphene Using Copper Catalyst. *Nano Lett.* **2010**, *10*, 4128–4133.

7. Han, G. H.; Güneş, F.; Bae, J. J.; Kim, E. S.; Chae, S. J.; Shin, H.-J.; Choi, J.-Y.; Pribat, D.; Lee, Y. H. Influence of Copper Morphology in Forming Nucleation Seeds for Graphene Growth. *Nano Lett.* **2011**, *11*, 4144–4148.

8. Luo, Z.; Lu, Y.; Singer, D. W.; Berck, M. E.; Somers, L. A.; Goldsmith, B. R.; Johnson, A. T. C. Effect of Substrate Roughness and Feedstock Concentration on Growth of Wafer-Scale Graphene at Atmospheric Pressure. *Chem. Mater.* **2011**, *23*, 1441–1447.

9. Liu, L.; Zhou, H.; Cheng, R.; Chen, Y.; Lin, Y.-C.; Qu, Y.; Bai, J.; Ivanov, I. A.; Liu, G.; Huang, Y. *et al.* A Systematic Study of Atmospheric Pressure Chemical Vapor Deposition Growth of Large-Area Monolayer Graphene. *J. Mater. Chem.* **2012**, *22*, 1498–1503.

10. Lee, Y.; Bae, S.; Jang, H.; Jang, S.; Zhu, S.-E.; Sim, S. H.; Song, Y. Il; Hong, B. H.; Ahn, J.-H. Wafer-Scale Synthesis and Transfer of Graphene Films. *Nano Lett.* **2010**, *10*, 490–493.

11. Lenski, D. R.; Fuhrer, M. S. Raman and Optical Characterization of Multilayer Turbostratic Graphene Grown *via* Chemical Vapor Deposition. *J. Appl. Phys.* **2011**, *110*, 013720.

12. Hu, B.; Ago, H.; Ito, Y.; Kawahara, K.; Tsuji, M.; Magome, E.; Sumitani, K.; Mizuta, N.; Ikeda, K.; Mizuno, S. Epitaxial Growth of Large-Area Single-Layer Graphene Over Cu(111)/Sapphire by Atmospheric Pressure CVD. *Carbon* **2012**, *50*, 57–65.

13. Vlassiouk, I.; Smirnov, S.; Ivanov, I.; Fulvio, P. F.; Dai, S.; Meyer, H.; Chi, M.; Hensley, D.; Datskos, P.; Lavrik, N. V Electrical and Thermal Conductivity of Low Temperature CVD Graphene: The Effect of Disorder. *Nanotechnology* **2011**, *22*, 275716.

14. Cao, H.; Yu, Q.; Jauregui, L. A.; Tian, J.; Wu, W.; Liu, Z.; Jalilian, R.; Benjamin, D. K.; Jiang, Z.; Bao, J. *et al.* Electronic Transport in Chemical Vapor Deposited Graphene Synthesized on Cu: Quantum Hall Effect and Weak Localization. *Appl. Phys. Lett.* **2010**, *96*, 122106.

15. Celebi, K.; Cole, M. T.; Teo, K. B. K.; Park, H. G. Observations of Early Stage Graphene Growth on Copper. *Electrochem. Solid St.* **2012**, *15*, K1–K4.

16. Huang, P. Y.; Ruiz-Vargas, C. S.; Zande, A. M. van der; Whitney, W. S.; Levendorf, M. P.; Kevek, J. W.; Garg, S.; Alden, J. S.; Hustedt, C. J.; Zhu, Y. *et al.* Grains and Grain Boundaries in Single-Layer Graphene Atomic Patchwork Quilts. *Nature* **2011**, *469*, 389–392.

17. Bae, S.; Kim, H.; Lee, Y.; Xu, X.; Park, J.-S.; Zheng, Y.; Balakrishnan, J.; Lei, T.; Ri Kim, H.; Song, Y. Il; *et al.* Roll-to-Roll Production of 30-inch Graphene Films for Transparent Electrodes. *Nat. Nanotechnol.* **2010**, *5*, 1–5.

18. Rasool, H. I.; Song, E. B.; Allen, M. J.; Wassei, J. K.; Kaner, R. B.; Wang, K. L.; Weiller, B. H.; Gimzewski, J. K. Continuity of Graphene on Polycrystalline Copper. *Nano Lett.* **2011**, *11*, 251–256.

19. Yu, V.; Whiteway, E.; Maassen, J.; Hilke, M. Straining Graphene by Chemical Vapour Deposition Growth on Copper. *arxiv.org* **2011**.

20. Li, X.; Cai, W.; An, J.; Kim, S.; Nah, J.; Yang, D.; Piner, R.; Velamakanni, A.; Jung, I.; Tutuc, E. *et al.* Large-Area Synthesis of High-Quality and Uniform Graphene Films on Copper Foils. *Science* **2009**, *324*, 1312–1314.

21. Zande, A. M. van der; Barton, R. A.; Alden, J. S.; Ruiz-Vargas, C. S.; Whitney, W. S.; Pham, P. H. Q.; Park, J.; Parpia, J. M.; Craighead, H. G.; McEuen, P. L. Large-Scale Arrays of Single-Layer Graphene Resonators. *Nano Lett.* **2010**, *10*, 4869–4873.

22. Vlassiouk, I.; Regmi, M.; Fulvio, P.; Dai, S.; Datskos, P.; Eres, G.; Smirnov, S. Role of Hydrogen in Chemical Vapor Deposition Growth of Large Single-Crystal Graphene. *ACS Nano* **2011**, *5*, 6069–6076.

23. Robertson, A. W.; Warner, J. H. Hexagonal Single Crystal Domains of Few-Layer Graphene on Copper Foils. *Nano Lett.* **2011**, *11*, 1182–1189.

24. Wu, B.; Geng, D.; Guo, Y.; Huang, L.; Xue, Y.; Zheng, J.; Chen, J.; Yu, G.; Liu, Y.; Jiang, L. *et al.* Equiangular Hexagon-Shape-Controlled Synthesis of Graphene on Copper Surface. *Adv. Mater.* **2011**, *23*, 3522–3525.

25. Li, X.; Magnuson, C. W.; Venugopal, A.; An, J.; Suk, J. W.; Han, B.; Borysiak, M.; Cai, W.; Velamakanni, A.; Zhu, Y. *et al.* Graphene Films with Large Domain Size by a Two-Step Chemical Vapor Deposition Process. *Nano Lett.* **2010**, *10*, 4328–4334.

26. Rasool, H. I.; Song, E. B.; Mecklenburg, M.; Regan, B. C.; Wang, K. L.; Weiller, B. H.; Gimzewski, J. K. Atomic-Scale Characterization of Graphene Grown on Copper (100) Single Crystals. *J. Am. Chem. Soc.* **2011**, *133*, 12536–12543.

27. Zhang, B.; Lee, W. H.; Piner, R.; Kholmanov, I.; Wu, Y.; Li, H.; Ji, H.; Ruoff, R. S. Low Temperature Chemical Vapor Deposition Growth of Graphene from Toluene on Electropolished Copper Foils. *ACS Nano* **2012**, *6*, 2471–2476.

28. Ohring, M. *Materials Science of Thin Films*; Second.; Academic Press: San Diego, 2002.

29. Bird, R. B.; Stewart, W. E.; Lightfoot, E. N. *Transport Phenomena*; John Wiley & Sons, Inc.: New York, 2002.

30. Norinaga, K.; Deutschmann, O.; Hüttinger, K. J. Analysis of Gas Phase Compounds in Chemical Vapor Deposition of Carbon from Light Hydrocarbons. *Carbon* **2006**, *44*, 1790–1800.

31. Olsvik, O.; Rokstad, O. A.; Holmen, A. Pyrolysis of Methane in the Presence of Hydrogen. *Chem. Eng. Technol.* **1995**, *18*, 349–358.